BROOKHAVEN
NATIONAL LABORATORY

BNL-113407-2017-JA

Polyvinylpyrrolidone induced anisotropic growth of gold nanoprisms in plasmon driven synthesis

Yueming Zhai, Joseph S. DuChene, Yi-Chung Wang, Jingjing Qiu, Aaron C. Johnston-Peck, Bo You, Wenxiao Gou, Benedetto DiCiaccio, Kun Qian, Evan W. Zhao, Frances Ooi, Dehong Hu, Dong Su, Eric A. Stach, Zihua Zhu and Wei David Wei

Submitted to Nature Materials

July 2016

Center for Functional Nanomaterials

Brookhaven National Laboratory

U.S. Department of Energy
USDOE Office of Science (SC),
Basic Energy Sciences (SC-22)

DISCLAIMER

Polyvinylpyrrolidone induced anisotropic growth of gold nanoprisms in plasmon driven synthesis

Yueming Zhai[1], Joseph S. DuChene[1], Yi-Chung Wang[1], Jingjing Qiu[1], Aaron C. Johnston-Peck[2], Bo You[1], Wenxiao Gou[1], Benedetto DiCiaccio[1], Kun Qian[1], Evan W. Zhao[1], Frances Ooi[1], Dehong Hu[3], Dong Su[2], Eric A. Stach[2], Zihua Zhu[3] and Wei David Wei[1]*

[1]Department of Chemistry and Center for Nanostructured Electronic Materials, University of Florida, Gainesville, Florida 32611, United States.

[2]Center for Functional Nanomaterials, Brookhaven National Laboratory, Upton, New York 11973, United States.

[3]Environmental Molecular Sciences Laboratory, Pacific Northwest National Laboratory, 3335 Q Avenue, Richland, Washington 99354, United States.

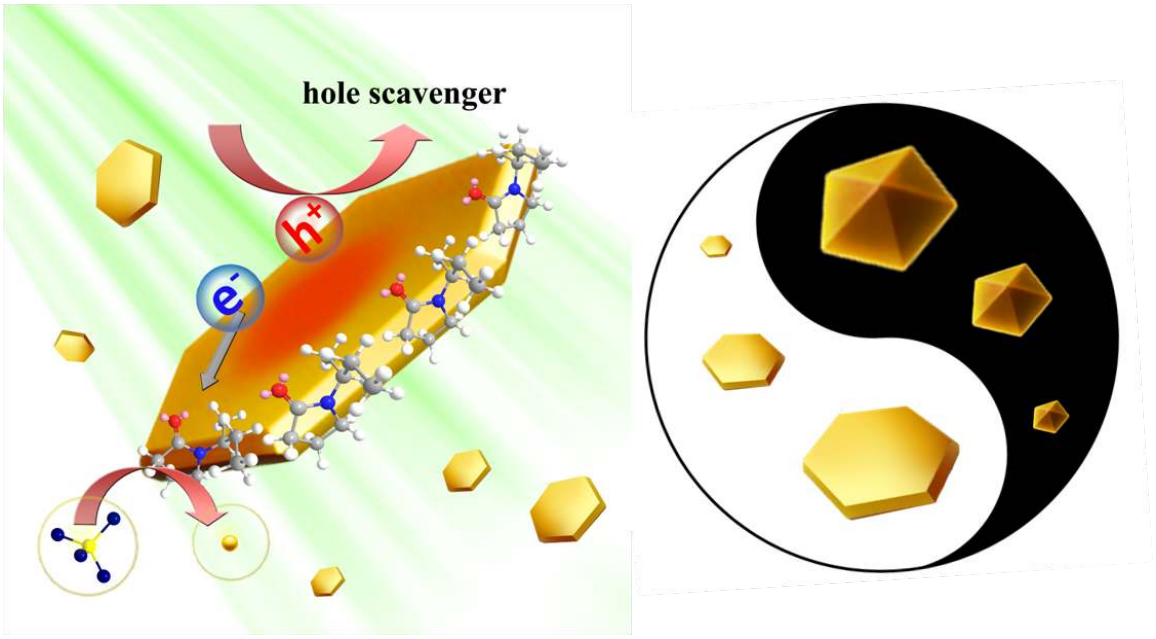

Abstract:

After more than a decade, it is still unknown whether the plasmon-mediated synthesis of silver nanostructures can be extended to the synthesis of other noble metals, as the molecular mechanisms governing the growth process remain elusive. Herein, we demonstrate the first plasmon-driven synthesis of gold nanoprisms and elucidate the details of the photochemical growth mechanism at the single-nanoparticle level. Our investigation reveals that the surfactant polyvinylpyrrolidone preferentially adsorbs along the nanoprism perimeter and serves as a photochemical relay to direct the anisotropic growth of gold nanoprisms. This discovery confers a unique function to polyvinylpyrrolidone that is fundamentally different from its widely accepted role as a crystal-face-blocking ligand. Additionally, we find that nanocrystal twinning exerts a profound influence on the kinetics of this photochemical process by controlling the transport of plasmon-generated hot electrons to polyvinylpyrrolidone. These insights establish a molecular-level description of the underlying mechanisms regulating the plasmon-driven synthesis of gold nanoprisms.

The prospect of wielding light as a tool for sculpting plasmonic-metal nanostructures has garnered immense scientific interest since the discovery of plasmon-mediated silver (Ag) nanoprism growth in 2001[1]. Unfortunately—despite more than a decade's worth of investigation—the scope of this photochemical strategy remains restricted solely to the synthesis of Ag-based nanostructures[2]. It is unknown whether this elemental exclusivity is indicative of a fundamental limitation of plasmonic photochemistry, or is merely a consequence of our insufficient understanding of the plasmon-driven process at the molecular level. Numerous studies have shown that the surface plasmon resonance (SPR) of the nanoparticle seeds must be excited to induce the irreversible photo-oxidation of adsorbed citrate molecules, which then facilitate the concomitant reduction of Ag precursors onto the metal nanocrystal[2-7]. It has been proposed that these photochemical reactions might be driven by highly energetic or "hot" electron-hole pairs produced via Landau damping during optical excitation of surface plasmons on the metal nanoparticle[2,3,6,7]. Although such a process may occur, a comprehensive description of the molecular mechanisms governing the evolution of anisotropic nanostructures from isotropic seeds remains elusive due to the chemical complexities inherent in the plasmon-mediated synthesis of Ag nanostructures[2,5,7-12].

Gold (Au) nanostructures are anticipated to provide an ideal system for exploring the plasmon-mediated growth process; they exhibit similar crystallographic structures and plasmonic properties to Ag nanostructures, but boast superior resistance to both chemical oxidation and electron-beam damage[13-16]. A mechanistic investigation of these photochemical reactions in nanomaterials composed of Au is therefore expected to lend

fundamental insight into this process and inform a more general description of plasmon-mediated nanocrystal growth. Additionally, the reduction potentials of commonly used Au precursors are less electrochemically demanding than those of Ag precursors ($AuCl_4^-$/Au: 0.99 V vs. SHE and Ag^+/Ag: 0.80 V vs. SHE)[17,18], suggesting that a similar photochemical pathway should occur in Au-based systems. However, to our surprise, the plasmon-driven synthesis of anisotropic Au nanostructures has yet to be achieved.

In this contribution, we expand the realm of noble metal nanostructures accessible via plasmonic photochemistry with the demonstration of plasmon-driven Au nanoprism synthesis. Growth studies at the single-nanoparticle level elucidate the mechanics of the plasmon-driven process and unambiguously clarify the anisotropic growth mechanism. Nanoscale secondary ion mass spectrometry (NanoSIMS)[19] was employed to probe the physical location of the surfactant polyvinylpyrrolidone (PVP) on individual Au nanostructures at the molecular level, revealing that it preferentially adsorbs onto twin-plane defects along the nanoprism perimeter instead of the top {111} facets as previously suggested. Electrochemical studies on Au nanocrystal electrodes further demonstrate that adsorbed PVP facilitates plasmon-driven charge separation, indicating that this surfactant performs a unique function as a photochemical relay to enable the anisotropic growth of Au nanoprisms from spherical Au seeds. These findings assign a new role to this ubiquitous surfactant that is distinct from its widely recognized function as a crystal-face-blocking ligand in nanomaterials synthesis. Further investigation showed that nanocrystal twinning itself regulates the transport of hot electrons under plasmon excitation, thereby modulating the photochemical growth kinetics of Au nanocrystals based upon their

intrinsic structural differences. These mechanistic insights inspired the development of a simple method for selectively producing hexagonal or triangular Au nanoprisms in high yield (~90%), demonstrating the general utility of plasmonic photochemistry for manipulating the growth of noble metal nanocrystals.

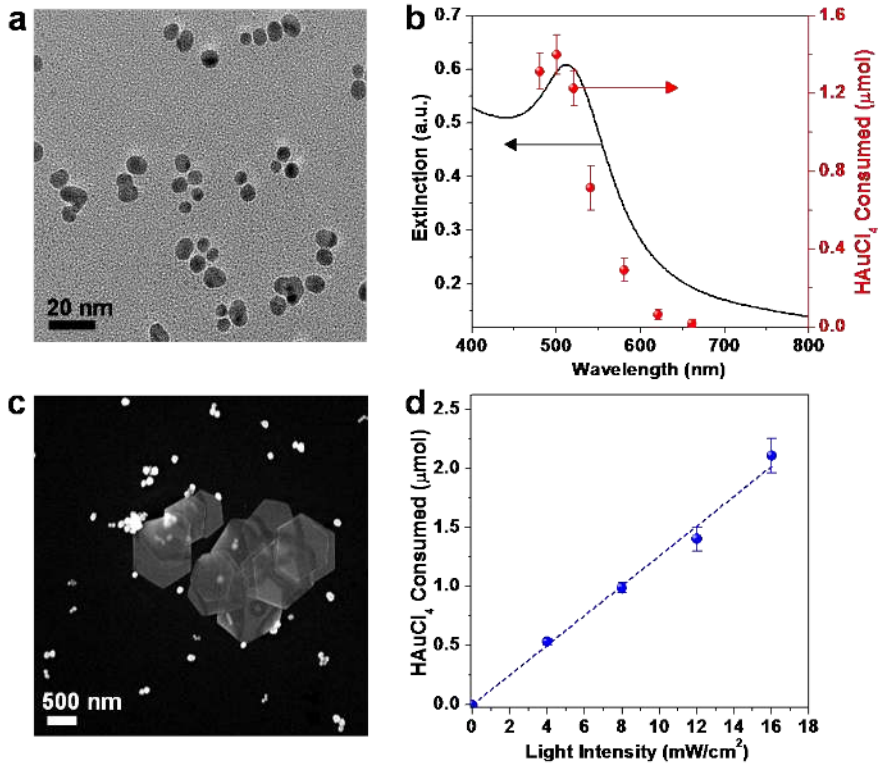

Figure 1 | Plasmon-driven synthesis of Au nanostructures. a, TEM image of the Au nanocrystals used as plasmonic seeds for the growth of Au nanostructures. **b,** Extinction spectrum of the Au seed solution (black curve) displaying a prominent SPR feature at 512 nm. The amount of Au precursor ($HAuCl_4$) consumed in the growth solution was correlated with the SPR of these seeds (red points) after 1 h of irradiation with various excitation wavelengths. **c**, SEM image of the final products obtained via irradiation of the growth solution with λ_{inc} = 500 ± 10 nm light for 2 h. **d**, Influence of incident light power

on the amount (μmol) of $HAuCl_4$ consumed in the growth solution during 1 h of irradiation (λ_{inc} = 500 ± 10 nm). All error bars in (**b**) and (**d**) indicate one standard deviation about the mean from three independent trials.

Pseudo-spherical Au nanoparticles with an average size of ca. 7 ± 3 nm (Fig. 1a) were used as seeds for the plasmon-driven growth of anisotropic Au nanoprisms (see Methods). The photochemical reaction was initiated by irradiating an aqueous growth solution containing the Au seeds, tetrachloroauric acid ($HAuCl_4$), PVP, and methanol with λ_{inc} = 500 ± 10 nm light to ensure that the incident excitation wavelength (λ_{inc}) was commensurate with the SPR of the Au seeds (Fig. 1b, black curve). Scanning electron microscopy (SEM) revealed that a mixture of Au nanoprisms and Au nanospheres were produced after 2 h of irradiation (Fig. 1c). The nanoprisms exhibit either triangular or hexagonal morphologies predominantly enclosed by {111} facets with an average edge length (l) of 496 ± 68 nm and an average thickness (h) of 22.0 ± 0.4 nm (Supplementary Fig. 1). The average diameter (d) of the Au nanospheres was 105 ± 14 nm. The photochemical growth process was monitored spectroscopically over the course of the 2 h reaction and correlated with the structural evolution of these Au nanocrystals via electron microscopy (Supplementary Fig. 2). The extinction spectra displayed the simultaneous emergence of two distinctive SPR features indicative of the concurrent growth of both pseudo-spherical nanoparticles (λ ~550 nm) and nanoprisms (λ ~1100 nm)[20]. Periodic inspection of the nanocrystal morphology by SEM demonstrates that both nanostructures evolve independently over the 2 h reaction (Supplementary Fig. 2 and Fig. 3). The

nanoprisms (both triangular and hexagonal) were obtained with a ca. 21% yield (by shape), consistent with the percentage of planar-twinned nanocrystals observed in the seed solution (Supplementary Fig. 4). Such a correlation confirms that nanoprism growth proceeds via a seed-mediated pathway[21,22]. Further investigation of the growth process shows that the reduction of $HAuCl_4$ increased linearly with the incident light intensity (Fig. 1d): this relationship is indicative of a photochemical reaction driven by visible light. A series of bandpass filters were then used to examine the influence of the incident wavelength (λ_{inc}) on the reduction of Au precursors ($HAuCl_4$). As shown in Fig. 1b (red points) and Supplementary Fig. 5, the visible-light-driven production of Au nanostructures was directly correlated with the optical properties of the Au seeds. These data confirm that SPR excitation of the Au nanocrystals is required to initiate the photochemical reaction.

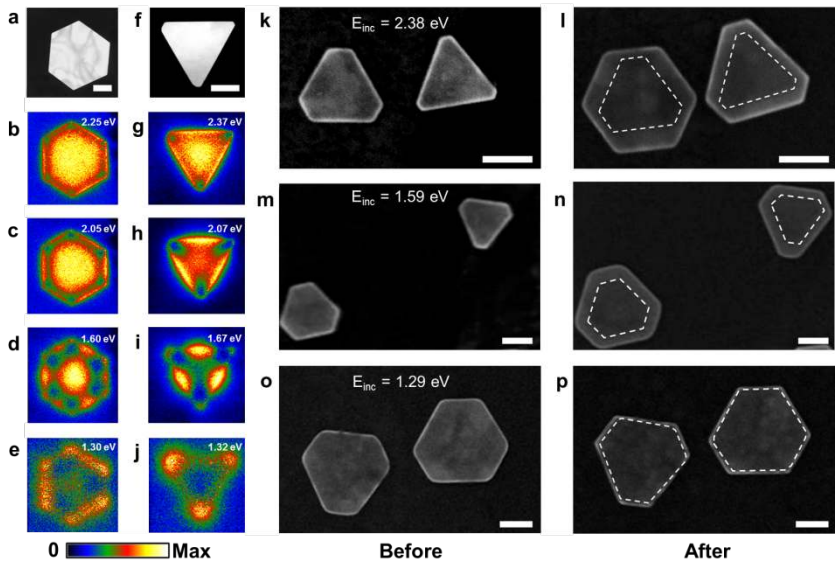

Figure 2 | The influence of plasmonic hot spots on Au nanoprism growth. a-e, ADF-STEM image with corresponding EELS maps acquired from a single Au hexagonal

nanoprism. **f-j,** ADF-STEM image with corresponding EELS maps acquired from a single Au triangular nanoprism. Scale bars in STEM images (**a**) and (**f**) also apply to their respective EELS maps. The common EELS intensity scale is linear and expressed in arbitrary units. **k-p,** SEM images of Au nanoprisms before irradiation (**k**, **m**, **o**) and after irradiation (**l**, **n**, **p**) with various excitation wavelengths (λ_{inc}) while immobilized on a Si substrate: (**k**, **l**) 520 nm, (**m**, **n**) 780 nm, (**o**, **p**) 960 nm. Dashed white lines indicate the initial Au nanoprism dimensions to aid comparison. All scale bars represent 100 nm.

It has long been suspected that the spatially inhomogeneous distribution of enhanced electromagnetic fields, or "hot spots," generated via plasmon excitation may direct the evolution of anisotropic Ag nanostructures from isotropic seeds[4,23]. We therefore examined this possibility in our Au system by using annular dark-field scanning transmission electron microscopy (ADF-STEM) in tandem with electron energy loss spectroscopy (EELS) to map the spatial distribution of plasmon modes on a single Au hexagonal nanoprism (Fig. 2, a to e) and a single Au triangular nanoprism (Fig. 2, f to j). These EELS maps depict the spatial variation of distinct plasmon modes along the nanoprisms, as the hot spots clearly shift from the center of the nanoprisms (~2.4 eV) to their perimeter (~1.3 eV) with decreasing energy (compare Fig. 2b to Fig. 2e). The influence of these hot spots on the nanostructure growth process was then investigated by monitoring the growth of individual nanoprisms immobilized on a silicon (Si) substrate while hot spots on different positions of these nanostructures were selectively excited with specific irradiation wavelengths (λ_{inc} = 520 nm, 780 nm, 960 nm). These

wavelengths were chosen to coincide with the optically accessible (i.e. bright) plasmon modes of the Au nanoprisms observable from the extinction spectrum[24]. Despite the anisotropic distribution of these different hot spots on the nanoprisms (Fig. 2, a to j), significant growth occurred only along the nanoprism perimeter (Fig. 2, k to p). Our finding is consistent with previous growth studies on Ag nanoparticles: isotropic nanocrystal growth was consistently observed despite manipulating the spatial orientation of the plasmonic hot spots by varying the incident light polarization[10]. This discrepancy between the near-field distribution and the nanoprism growth direction clearly demonstrates that the anisotropic morphology is not determined by the spatial distribution of these plasmonic hot spots.

Although the possibility of local photothermal heating must be considered in a plasmon-driven reaction[2], the excellent thermal conductivity of Au ensures that an isotropic temperature distribution is rapidly (~ps–ns) established on the entire nanoparticle surface[25]. This thermal uniformity renders such a process incapable of promoting the anisotropic growth of nanoprisms. Since the bulk solution temperature measured under low-power continuous light irradiation (32 °C after 2 h) can be used as a surrogate for the nanoparticle surface temperature[26], the growth solution was incubated at 32 °C in the dark for 2 h to assess a potential photothermal contribution; however, no detectable growth was observed (Supplementary Fig. 6). It is further noted that the linear relationship observed between the plasmon-driven reduction of $HAuCl_4$ and the incident light intensity (Fig. 1d) is the signature of an electron-driven photochemical reaction, rather than a photothermal process[4,27].

Taken together, these observations strongly suggest that the plasmon-mediated production of hot electron-hole pairs drives the photochemistry necessary for nanomaterials growth. The hot holes should be quickly scavenged by the sacrificial reagent methanol, which is oxidized to yield formaldehyde as a photochemical byproduct (Supplementary Fig. 7). Hot electrons then readily reduce Au precursors from solution to enable the plasmon-driven growth of Au nanostructures while. However, it is unlikely that these hot electrons can directly reduce the Au precursors due to the incommensurate timescales between the hot electron lifetime (~fs–ps)[8,28] and the slow kinetics of $HAuCl_4$ reduction (~μs–ms)[29]. This plasmon-driven photocatalytic model therefore requires an intervening chemical species adsorbed on the Au nanoparticle surface that can prolong their lifetime and foster the multi-electron reduction of $HAuCl_4$. A cursory examination of our growth solution composition implies that the surfactant PVP is the only constituent capable of performing the aforementioned function (Supplementary Fig. 7 and Fig. 8). It must be noted that PVP itself is incapable of directly reducing the Au precursor under our experimental conditions (Supplementary Fig. 9). Further experiments show that the surface charge of PVP is dependent upon solution pH (Supplementary Fig. 10) and that Au nanoprisms were only observed when a positive surface charge was imparted to PVP by the acidic (pH 3) growth solution (Supplementary Fig. 11). It is also noted that Au nanoprisms grow if the PVP monomer (*N*-methyl-2-pyrrolidone) is substituted for the polymer (Supplementary Fig. 12), indicating that the γ-lactam ring comprises the critical chemical moiety in PVP that enables anisotropic growth. All these results suggest that PVP could fulfill a complementary role in the plasmon-driven process: the electrostatic

force from positively-charged PVP molecules would induce the formation of an electrical adlayer on the Au nanocrystal surface capable of coulombically attracting hot electrons generated via plasmon excitation. Additionally, this positively-charged adlayer should permit PVP molecules to capture negatively-charged Au precursors ($AuCl_4^-$) from solution and form a PVP-metal complex for facilitating reduction reactions on the Au nanostructure surface[30].

Electrochemical evidence for the direct involvement of PVP in the plasmon-driven growth of Au nanoprisms is obtained by monitoring the open-circuit voltage (V_{oc}) of Au nanocrystal electrodes under visible-light irradiation (see Methods). As the photovoltage ($V_{ph} = V_{oc,\ light} - V_{oc,\ dark}$) established under steady-state conditions corresponds to the accumulation of hot electrons within the Au nanocrystals, chronopotentiometry[10,31] was used to assess the ability for adsorbed PVP molecules to participate in plasmon-driven photochemistry. Upon exposure to visible-light irradiation ($\lambda_{inc} > 495$ nm), a prompt rise in photovoltage (V_{ph} ~28 mV) was observed from the Au nanoparticles functionalized with PVP, while only a modest photovoltage (V_{ph} ~6 mV) was established in the absence of this surfactant (Supplementary Fig. 13). These results demonstrate that adsorbed PVP molecules assist with the accumulation of hot electrons on the Au nanocrystals.

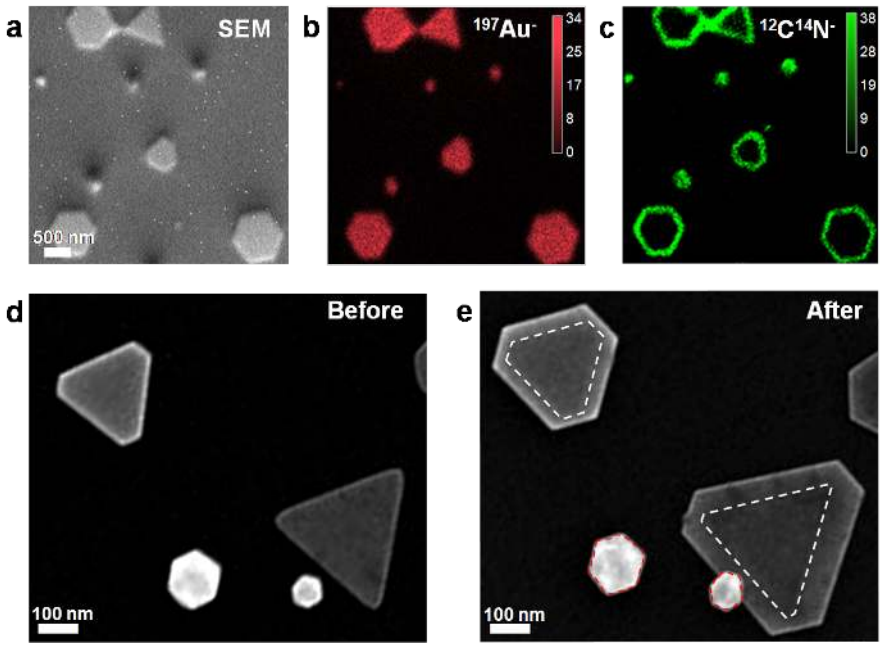

Figure 3 | The role of PVP in directing the anisotropic growth of Au nanoprisms. **a,** SEM image of Au nanostructures obtained after 2 h of photochemical growth. **b**,**c**, NanoSIMS images obtained from the Au nanostructures in (**a**) showing the elemental distributions of $^{197}Au^-$ (red) signals (**b**) and $^{12}C^{14}N^-$ (green) signals (**c**). The scale bar in (**a**) also applies to images (**b**) and (**c**). **d**,**e**, SEM images of individual Au nanoprisms and pseudo-spherical nanoparticles before growth (**d**) and after growth (**e**) under λ_{inc} = 500 ± 10 nm light irradiation for 30 min. Dashed white and red lines indicate the initial dimensions of the nanoprisms and nanoparticles, respectively.

This proposed function for PVP implies that the physical location of this surfactant should play a critical role in determining the anisotropic growth of the Au nanoprisms. Accordingly, NanoSIMS was used to probe the spatial distribution of PVP molecules on

individual Au nanoprisms (Fig. 3, a to c). As shown in Fig. 3c, $^{12}C^{14}N^-$ signals attributable to adsorbed PVP molecules were primarily detected from the perimeters of the nanoprisms rather than their top {111} facets, while $^{12}C^{14}N^-$ signals were observed from the entire surface of the pseudo-spherical nanoparticles. This discovery is striking, as it shows that PVP is serving a distinct function from its widely accepted role as a crystal-face-blocking ligand in shape-controlled nanomaterials synthesis[21,32-36]. Instead, these NanoSIMS results reinforce our proposed role for PVP as an electrochemical relay. The adsorption of positively-charged PVP molecules constitutes an electrical adlayer along the Au nanoprism perimeter; this formed PVP-Au interface facilitates charge separation by coulombically attracting the hot electrons produced via optical excitation to the nanoprism edge. Meanwhile, the positively-charged electrical adlayer also interacts with negatively-charged Au precursors ($AuCl_4^-$) in solution to form a surfactant-metal precursor complex[30] along the nanoprism perimeter. Thus, these two functions cooperatively couple hot electrons with Au precursors to preferentially promote lateral growth and facilitate the formation of anisotropic Au nanoprisms (Fig. 1c). It is noted that only irregularly-shaped Au nanostructures were obtained when PVP was excluded from the growth solution (Supplementary Fig. 14), demonstrating that this surfactant performs an integral function in regulating the structural evolution of anisotropic Au nanoprisms from isotropic seeds.

To further confirm that PVP dictates the direction of Au nanostructure growth, an increased amount of PVP (20 times more) was used in the growth solution to promote adsorption onto the top and bottom {111} facets and induce vertical growth. As expected,

thicker (h = 49 ± 8 nm) Au nanoprisms were obtained with increased PVP concentrations (Supplementary Fig. 15). Subsequent inspection of these nanoprisms with NanoSIMS revealed the adsorption of PVP onto their top {111} facets with increased surfactant concentrations, as $^{12}C^{14}N^-$ signals were observed from the entire surface of the Au nanoprisms (Supplementary Fig. 16). These results confirm that PVP is performing a unique function as a photocatalytic intermediary, directing the growth trajectory of Au nanostructures by sequestering the hot electrons produced via plasmon excitation at the nanoprism perimeter where they catalyze the reduction of $AuCl_4^-$ ions and preferentially promote lateral growth.

The twin planes exposed along the nanoprism perimeter exhibit structural defects such as kinks, steps, and high-index facets (Supplementary Fig. 17) that impart increased surface energies to these unique structural sites[21,33,37]. It has been reported that these defects prompt surfactant adsorption to minimize the surface energy of the metal nanocrystal[38], as confirmed by the occurrence of $^{12}C^{14}N^-$ signals from adsorbed PVP molecules covering the entire surface of the multiply-twinned nanoparticles (Fig. 3c). Thus, these twin-plane defects capped with PVP serve as the reactive sites for nanomaterials growth.

Since hot electrons are known to exhibit substantial mean free paths (l_{mfp} ~150 nm) in Au nanostructures[39], their transport to the active site is anticipated to constitute a critical step in the plasmon-driven growth mechanism. The inconsistency observed between the physical locations of plasmonic hot spots and the nanoprism growth direction (Fig. 2) implies that these hot electrons must travel significant distances along

the Au nanocrystals prior to catalyzing the reduction of $AuCl_4^-$ species. The ballistic mean free path l_{mfp} of hot electrons can be hindered by scattering off crystal defects, phonons, impurities, etc., with the various contributions adding together according to Matthiessen's rule: $(l_{mfp})^{-1} = (l_{defect})^{-1} + (l_{phonon})^{-1} + (l_{impurity})^{-1} + \ldots$[25,40]. Thus, twin-plane defects within the Au nanocrystals are anticipated to attenuate the mean free path of these hot electrons by increasing their scattering rate, which ultimately lowers the overall photochemical quantum yield of the reaction[25,41]. The hot electrons within the planar-twinned nanocrystals should be scattered less than those within the multiply-twinned nanocrystals, and thereby accumulate more readily under optical excitation. Indeed, open-circuit photovoltage measurements demonstrate that the planar-twinned nanoprisms exhibit a much larger photovoltage (V_{ph} ~60 mV) under visible-light irradiation (λ_{inc} > 495 nm) than that of the multiply-twinned nanocrystals (V_{ph} ~30 mV) (Supplementary Fig. 22). Single-nanoparticle growth studies further revealed that the penta-twinned nanoparticles displayed minimal growth under optical excitation, while the increased size of the planar-twinned nanoprisms was clearly evident (Fig. 3, d and e). This observation indicates that SPR excitation manipulates the growth rate of the Au seeds based upon their internal crystal structure. Further analysis of the growth kinetics at the single-nanoparticle level (Supplementary Fig. 18 to 21) unambiguously reveals the pivotal role of plasmon excitation in preferentially promoting the reaction rate of the planar-twinned nanostructures relative to their multiply-twinned counterparts (Supplementary Table 1).

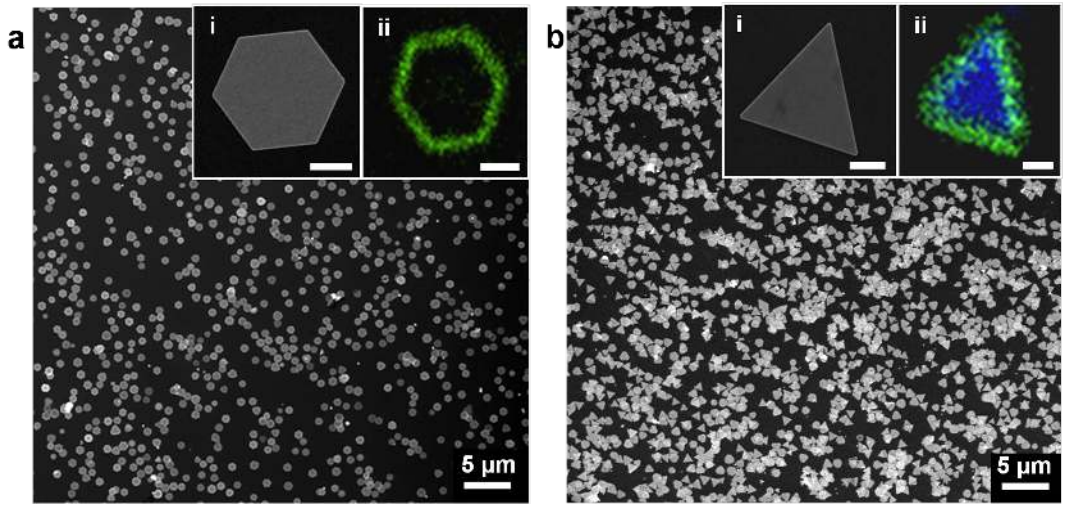

Figure 4 | Plasmon-driven synthesis of Au nanoprisms in high purity. a, SEM image of Au hexagonal nanoprisms obtained via the seed separation method. The insets show (**i**) a high-magnification SEM image of a single hexagonal nanoprism and (**ii**) a NanoSIMS image showing the elemental distribution of $^{12}C^{14}N^-$ signals (green) from adsorbed PVP on a hexagonal nanoprism. **b**, SEM image of Au triangular nanoprisms obtained via the seed separation method with the addition of iodide (I^-). The insets show (**i**) a high-magnification SEM image of a single triangular nanoprism and (**ii**) a NanoSIMS image showing the elemental distribution of $^{12}C^{14}N^-$ signals (green) and $^{127}I^-$ signals (blue) from a triangular nanoprism. The scale bars in all insets represent 200 nm.

The ability to modulate the growth kinetics of structurally distinct Au nanocrystals via SPR excitation inspired the development of a novel seed separation strategy for selectively preparing planar-twinned Au nanoprisms (see Supplementary Scheme 1). To date, the synthesis of planar-twinned Au nanostructures in high yields remains challenging due to the diverse distribution of nanocrystal structures present in the initial

seed solution[22,42-44]. Here, we exploit the disparate growth kinetics of different twinned nanocrystals to separate the Au seeds based upon their intrinsic structural characteristics (Supplementary Table 1). The growth solution was first incubated in the dark to preferentially enlarge the multiply-twinned seeds, while rendering the planar-twinned seeds relatively unreactive as their growth rates are vastly reduced in the dark (Supplementary Fig. 20 and Fig. 21). These multiply-twinned nanoparticles were then large enough (d > 100 nm) to be easily separated from the planar-twinned seeds (d ~15 nm) by centrifugation (Supplementary Fig. 20). The supernatant, now highly enriched with planar-twinned nanocrystals (Supplementary Fig. 23), was then irradiated to produce Au hexagonal nanoprisms in exceptionally high yield (~90%), as shown in Fig. 4a and Supplementary Fig. 24. The monodisperse nature of the final products was also confirmed by UV-Vis spectroscopy (Supplementary Fig. 25), demonstrating the utility of this unique synthetic approach for producing planar-twinned Au nanoprisms in excellent purity. Additional architectural control was achieved through the inclusion of iodide to the growth solution (20 μM NaI), which allowed the production of Au triangular nanoprisms with sharp tips (Fig. 4b and Fig. 4bi). Inspection of these nanoprisms by NanoSIMS revealed that $^{127}I^-$ (blue) was distributed across the entire {111} surface (Fig. 4bii and Supplementary Fig. 26), while $^{12}C^{14}N^-$ signals (green) from adsorbed PVP were still obtained along the triangular nanoprism perimeter (Fig. 4bii). These results are consistent with previous growth studies suggesting that iodide promotes triangular nanoprism growth by passivating Au {111} facets[22,43-45]. Such clear delineation between the adsorption locations of these two distinct surface species highlights the merits of

combining complementary capping agents to tune nanocrystal growth via this plasmon-driven synthesis strategy.

These findings significantly broaden the scope of noble metal architectures accessible by plasmonic photochemistry through the realization of plasmon-driven Au nanoprism synthesis. Systematic evaluation of the growth mechanism at the single-nanoparticle level reveals that the surfactant PVP serves as a photochemical relay to direct the evolution of anisotropic Au nanoprisms from pseudo-spherical Au seeds: preferential adsorption of PVP onto twin boundaries along the nanocrystal perimeter promotes lateral growth by coupling the photo-generated hot electrons produced on the nanoparticle surface with gold precursors in solution. Our studies elucidate the critical role of adsorbed surface molecules in plasmonic photochemistry, conferring additional chemical functionality to surfactants in the plasmon-driven synthesis of noble metal nanostructures. Further growth studies on individual nanoparticles exposed that nanocrystal twinning regulates the reduction kinetics of the plasmon-driven process, revealing a new route to manipulate photochemical reactions via the intrinsic structural features of the nanocrystal itself. This insight inspired a strategy for exploiting SPR excitation to selectively express the planar-twinned seed morphology and produce hexagonal or triangular Au nanoprisms in high yield (~90%). Taken together, these studies elucidate the fundamental physicochemical processes that regulate the plasmon-driven synthesis of noble metal nanostructures at the molecular level and illustrate the importance of collectively controlling the interaction among light, surfactants, and nanocrystal twinning to effectively harness plasmon-driven photochemistry for

nanomaterials synthesis (Supplementary Figure S27).

References and Notes:

1. Jin, R. *et al.* Photoinduced conversion of silver nanospheres to nanoprisms. *Science* **294**, 1901-1903 (2001).
2. Langille, M. R., Personick, M. L. & Mirkin, C. A. Plasmon-mediated syntheses of metallic nanostructures. *Angew. Chem. Int. Ed.* **52**, 13910-13940 (2013).
3. Xue, C., Millstone, J. E., Li, S. & Mirkin, C. A. Plasmon-driven synthesis of triangular core–shell nanoprisms from gold seeds. *Angew. Chem. Int. Ed.* **46**, 8436-8439 (2007).
4. Maillard, M., Huang, P. & Brus, L. Silver nanodisk growth by surface plasmon enhanced photoreduction of adsorbed [Ag^{+}]. *Nano Lett.* **3**, 1611-1615 (2003).
5. Xue, C., Metraux, G. S., Millstone, J. E. & Mirkin, C. A. Mechanistic study of photomediated triangular silver nanoprism growth. *J. Am. Chem. Soc.* **130**, 8337-8344 (2008).
6. Wu, X. *et al.* Photovoltage mechanism for room light conversion of citrate stabilized silver nanocrystal seeds to large nanoprisms. *J. Am. Chem. Soc.* **130**, 9500-9506 (2008).
7. Langille, M. R., Zhang, J., Personick, M. L., Li, S. & Mirkin, C. A. Stepwise evolution of spherical seeds into 20-fold twinned icosahedra. *Science* **337**, 954-957 (2012).
8. Watanabe, K., Menzel, D., Nilius, N. & Freund, H. J. Photochemistry on metal nanoparticles. *Chem. Rev.* **106**, 4301-4320 (2006).
9. Chen, H., Ratner, M. A. & Schatz, G. C. QM/MM Study of photoinduced reduction of a tetrahedral Ag_{20}^{+} cluster by a Ag atom. *J. Phys. Chem. C* **118**, 1755-1762 (2012).
10. Redmond, P. L., Wu, X. & Brus, L. Photovoltage and photocatalyzed growth in citrate-stabilized colloidal silver nanocrystals. *J. Phys. Chem. C* **111**, 8942-8947 (2007).
11. Jin, R. *et al.* Controlling anisotropic nanoparticle growth through plasmon excitation. *Nature* **425**, 487-490 (2003).
12. Lee, G. *et al.* Light-driven transformation processes of anisotropic silver nanoparticles. *ACS Nano* **7**, 5911-5921 (2013).
13. Zhai, Y. *et al.* Superparamagnetic plasmonic nanohybrids: shape-controlled synthesis, TEM-induced structure evolution, and efficient sunlight-driven inactivation of bacteria. *ACS Nano* **5**, 8562-8570 (2011).
14. Alloyeau, D. *et al.* Unravelling kinetic and thermodynamic effects on the growth of gold nanoplates by liquid transmission electron microscopy. *Nano Lett.* **15**, 2574-2581 (2015).
15. Lee, K. E., Hesketh, A. V. & Kelly, T. L. Chemical stability and degradation mechanisms of triangular Ag, Ag@Au, and Au nanoprisms. *Phys. Chem. Chem. Phys.* **16**, 12407-12414 (2014).
16. Behzad, T. *et al.* Triangular gold nanoplate growth by oriented attachment of Au seeds generated by strong field laser reduction. *Nano Lett.* **15**, 3377-3382 (2015).
17. Lide, D. R. *CRC Handbook of Chemistry and Physics* (CRC Press/Taylor and Francis: Boca Raton, Florida, 2008).
18. Yang, Y., Liu, J., Fu, Z. & Qin, D. Galvanic replacement-free deposition of Au on Ag for core–shell nanocubes with enhanced chemical stability and SERS activity. *J. Am.*

Chem. Soc. **136**, 8153-8156 (2014).
19. Senoner, M. & Unger, W. E. S. SIMS imaging of the nanoworld: applications in science and technology. *J. Anal. At. Spectrom.* **27**, 1050-1068 (2012).
20. Millstone, J. E. *et al.* Observation of a quadrupole plasmon mode for a colloidal solution of gold nanoprisms. *J. Am. Chem. Soc.* **127**, 5312-5313 (2005).
21. Xia, Y., Xiong, Y., Lim, B. & Skrabalak, S. E. Shape-controlled synthesis of metal nanocrystals: simple chemistry meets complex physics? *Angew. Chem. Int. Ed.* **48**, 60-103 (2009).
22. DuChene, J. S. *et al.* Halide anions as shape-directing agents for obtaining high-quality anisotropic gold nanostructures. *Chem. Mater.* **25**, 1392-1399 (2013).
23. Paul, A., Kenens, B., Hofkens, J. & Uji-i, H. Excitation polarization sensitivity of plasmon-mediated silver nanotriangle growth on a surface. *Langmuir* **28**, 8920-8925 (2012).
24. Koh, A. L., Bao, K., Khan, I., Smith, W. E., Kothleitner, G., Nordlander, P., Maier, S. A. & McComb, D. W. Electron energy-loss spectroscopy (EELS) of surface plasmons in single silver nanoparticles and dimers: influence of beam damage and mapping of dark modes. *ACS Nano* **3**, 3015-3022 (2009).
25. Hartland, G. V. Optical studies of dynamics in noble metal nanostructures. *Chem. Rev.* **111**, 3858-3887 (2011).
26. Govorov, A. O. *et al.* Gold nanoparticle ensembles as heaters and actuators: melting and collective plasmon resonances. *Nanoscale Res. Lett.* **1**, 84-90 (2006).
27. Linic, S., Aslam, U., Boerigter, C. & Morabito, M. Photochemical transformations on plasmonic metal nanoparticles. *Nat. Mater.* **14**, 567-576 (2015).
28. Manjavacas, A., Liu, J. G., Kulkarni, V. & Nordlander, P. Plasmon-induced hot carriers in metallic nanoparticles. *ACS Nano* **8**, 7630-7638 (2014).
29. Polte, J. *et al.* Nucleation and growth of gold nanoparticles studied via in situ small angle X-ray scattering at millisecond time resolution. *ACS Nano* **4**, 1076-1082 (2010).
30. Regalbuto, J. R. *Catalyst Preparation: Science and Engineering* (CRC Press/Taylor and Francis Group, 2007).
31. Wu, X., Thrall, E. S., Liu, H., Steigerwald, M. & Brus, L. Plasmon induced photovoltage and charge separation in citrate-stabilized gold nanoparticles. *J. Phys. Chem. C* **114**, 12896-12899 (2010).
32. Zeng, J. *et al.* Successive deposition of silver on silver nanoplates: lateral versus vertical growth. *Angew. Chem. Int. Ed.* **50**, 244-249 (2011).
33. Millstone, J. E., Hurst, S. J., Métraux, G. S., Cutler, J. I. & Mirkin, C. A. Colloidal gold and silver triangular nanoprisms. *Small* **5**, 646-664 (2009).
34. Tao, A. R., Habas, S. & Yang, P. Shape control of colloidal metal nanocrystals. *Small* **4**, 310-325 (2008).
35. Xia, Y., Xia, X. & Peng, H. Shape-controlled synthesis of colloidal metal nanocrystals: thermodynamic versus kinetic products. *J. Am. Chem. Soc.* **137**, 7947-7966 (2015).
36. Li, J., Liu, J., Yang, Y. & Qin, D. Bifunctional Ag@Pd-Ag nanocubes for highly sensitive monitoring of catalytic reactions by surface-enhanced Raman spectroscopy. *J. Am. Chem. Soc.* **137**, 7039-7042 (2015).

37. Wang, Y. M. *et al.* Defective twin boundaries in nanotwinned metals. *Nat. Mater.* **12**, 697-702 (2013).
38. Saywell, A., Schwarz, J., Hecht, S. & Grill, L. Polymerization on stepped surfaces: alignment of polymers and identification of catalytic sites. *Angew. Chem. Int. Ed.* **51**, 5096-5100 (2012).
39. McFarland, E. W. & Tang, J. A photovoltaic device structure based on internal electron emission. *Nature* **421**, 616-618 (2003).
40. Redmond, P. L. & Brus, L. E. "Hot electron" photo-charging and electrochemical discharge kinetics of silver nanocrystals. *J. Phys. Chem. C* **111**, 14849-14854 (2007).
41. Lu, L., Shen, Y., Chen, X., Qian, L. & Lu, K. Ultrahigh strength and high electrical conductivity in copper. *Science* **304**, 422-426 (2004).
42. Personick, M. L., Langille, M. R., Wu, J. & Mirkin, C. A. Synthesis of gold hexagonal bipyramids directed by planar-twinned silver triangular nanoprisms. *J. Am. Chem. Soc.* **135**, 3800-3803 (2013).
43. Scarabelli, L., Coronado-Puchau, M., Giner-Casares, J. J., Langer, J. & Liz-Marzán, L. M. Monodisperse gold nanotriangles: size control, large-scale self-assembly, and performance in surface-enhanced Raman scattering. *ACS Nano* **8**, 5833-5842 (2014).
44. Chen, F. *et al.* High-yield seedless synthesis of triangular gold nanoplates through oxidative etching. *Nano Lett.* **14**, 7201-7206 (2014).
45. Millstone, J. E., Wei, W., Jones, M. R., Yoo, H. & Mirkin, C. A. Iodide ions control seed-mediated growth of anisotropic gold nanoparticles. *Nano Lett.* **8**, 2526-2529 (2008).

Acknowledgments

The work is supported by the Air Force Office of Scientific Research under AFOSR Award No. FA9550-14-1-0304. We also thank the National Science Foundation for support under Grant CHE-1308644 and the CCI Center for Nanostructured Electronic Materials (CHE-1038015). F. Ooi and B. DiCiaccio acknowledge the generous support from the University of Florida (UF) Howard Hughes Medical Institute (HHMI) Intramural Award and the UF University Scholars Program. B. You acknowledges support from UF's Student Science Training Program. We thank M. Hill and Dr. B. Sumerlin for assistance with Zeta potential measurements. Electron microscopy work was carried out in part at the Center for Functional Nanomaterials at Brookhaven National Laboratory (Upton, NY) through User Proposal BNL-CFN-31913 and BNL-

CFN-33789, supported by the U.S. Department of Energy (DOE), Office of Basic Energy Sciences, under Contract DE-SC0012704. A portion of the research (AFM and NanoSIMS characterization) was performed at the Environmental Molecular Sciences Laboratory (EMSL) through User Proposal 40065, a national scientific user facility sponsored by the DOE Office of Biological and Environmental Research and located at Pacific Northwest National Laboratory (PNNL) (Richland, WA). PNNL is operated by Battelle for the U.S. DOE under contract DE-AC06-76RLO1930.

Author Contributions Y.Z., J.S.D., and W.D.W. conceived the system and designed the experiments. Y.Z., B.Y., and W.G. synthesized the materials. J.S.D., A.C.J-P., D.S., and E.A.S. performed the EELS and TEM characterization. Y.W. and Z.Z. performed the NanoSIMS characterization. Y.Z., J.Q., and E.W.Z. performed the SEM measurements. Y.W. and D.H. performed the AFM measurement. Y.Z., J.S.D., and W.D.W. analyzed and interpreted the data. Y.Z., J.S.D., and W.D.W. prepared the manuscript with contributions from all authors. W.D.W. supervised the project. All authors contributed to discussions.

Author Information Supplementary Information is available in the online version of the paper. Reprints and permissions information is available at www.nature.com/reprints. Readers are welcome to comment on the online version of the paper. Correspondence and requests for materials should be addressed to W.D.W. (wei@chem.ufl.edu).

Competing financial interests

The authors declare no competing financial interests.

Methods

Synthesis of Au nanoprisms

Pseudo-spherical Au seeds were prepared according to a previously described method[22]. A photochemical growth solution was prepared by adding 5 mg of PVP to a mixture of 10 mL Nanopure™ H_2O and 1 mL methanol. Then, 0.8 mL of a 10 mM $HAuCl_4$ aqueous solution and 2 μL of the above-mentioned Au seed solution were added into the mixture and gently mixed. For the growth of triangular Au nanoprisms, 20 μL of 10 mM NaI was also added to this solution. The growth solution was illuminated for 2 h with a halogen lamp (Dolan Jenner, Model No. MI-150) equipped with a bandpass filter (Thor Labs, Inc.) under an incident power of I_0 ~12 mW/cm^2 on the sample surface. The standard growth protocol involved the use of a 500 ± 10 nm bandpass filter. For wavelength-dependent growth experiments, the solution was illuminated with various bandpass filters from λ_{inc} = 480–660 nm, each exhibiting a bandwidth (FWHM) of 10 ± 2 nm. Nanostructure growth products were collected after synthesis by centrifugation at 5,000 rpm for 5 min and redispersed in Nanopure™ H_2O. This procedure was repeated two more times to remove excess surfactants from the nanostructure surface before characterization of the samples by electron microscopy.

Single-nanoparticle growth experiments conducted on a Si substrate

Smaller Au nanoprisms and Au nanospheres were obtained using the above-described synthetic method with a shorter irradiation time. After the reaction these products were centrifuged and washed with Nanopure™ H_2O three times. The nanostructures were then immobilized on the Si substrate by drop-casting a small aliquot onto the substrate and allowing it to thoroughly dry in a desiccator. The substrate was then immersed in a fresh growth solution (as prepared above) to conduct further experiments under dark or light conditions. All Si substrates were marked to provide a means of inspecting an individual nanocrystal before growth commenced and then relocating the same nanostructure after the reaction was ceased. This approach enabled the observation of the growth trajectories of individual Au nanoparticles. For comparison with the hot spot distribution observed from the EELS maps, the samples were illuminated for 30 min under the following incident wavelengths: λ_{inc} = 520 ± 10 nm (~2.4 eV), λ_{inc} = 780 ± 10 nm (~1.6 eV), or λ_{inc} = 960 ± 10 nm (~1.3 eV). The substrate was illuminated for 30 min with a halogen lamp (Dolan Jenner, Model No. MI-150) equipped with a bandpass filter (Thor Labs, Inc.) under an incident power of I_0 ~12 mW/cm^2 on the sample surface.

Electrochemistry

Electrochemical experiments were conducted via the construction of a three-electrode electrochemical cell controlled by a potentiostat (EC Epsilon, Bioanalytical Systems, Inc.) with a Au nanocrystal working photoelectrode, a Pt wire auxiliary electrode, and a Ag/AgCl reference electrode all immersed in a supporting electrolyte of 0.1 M $NaSO_4$

with 10% (vol%) methanol (tuned to pH 3.0 via HCl addition). The Au nanocrystal photoelectrodes were prepared as follows: Au nanoparticles without PVP were first obtained via UV-light irradiation (λ_{inc} = 280–400 nm) of an aqueous $HAuCl_4$ solution to photochemically reduce this metal precursor directly into Au nanoparticles in the absence of any surfactants. These Au nanoparticles were then deposited onto the fluorine-doped tin oxide (FTO) glass substrate by drop-casting and subsequent heating at 150 °C for 20 min to ensure sufficient adhesion with the underlying substrate. The working electrode area was 2 cm^2. The photoanode was illuminated through the FTO glass substrate with an ozone-free 300 W Xe lamp (Newport Corp.) equipped with a 495 nm longpass filter (Newport Corp.) under an incident power of I_0 ~1.5 W/cm^2. To modify the nanocrystals with PVP, the exact same Au nanoparticle electrode was then dipped into an aqueous solution containing 5 mg/mL PVP for 10 min to allow PVP adsorption. The Au nanoparticle electrode (now functionalized with PVP molecules) was then copiously rinsed with Nanopure™ H_2O to remove any molecules not specifically bound to the Au nanoparticles. The photoelectrode was then illuminated under identical conditions as before to provide a direct comparison of the photovoltage obtained from the exact same Au nanoparticle electrode with and without PVP.

Supporting Information

Polyvinylpyrrolidone Determines Anisotropic Growth in the Plasmon-Driven Synthesis of Gold Nanoprisms

Yueming Zhai[1], Joseph S. DuChene[1], Yi-Chung Wang[1], Jingjing Qiu[1], Aaron C. Johnston-Peck[2], Bo You[1], Wenxiao Gou[1], Benedetto DiCiaccio[1], Kun Qian[1], Evan W. Zhao[1], Frances Ooi[1], Dehong Hu[3], Dong Su[2], Eric A. Stach[2], Zihua Zhu[3], and Wei David Wei[*1]

[1]Department of Chemistry and Center for Nanostructured Electronic Materials, University of Florida, Gainesville, Florida 32611, United States
[2]Center for Functional Nanomaterials, Brookhaven National Laboratory, Upton, New York 11973, United States
[3]Environmental Molecular Sciences Laboratory, Pacific Northwest National Laboratory, 3335 Q Avenue, Richland, Washington 99354, United States
[*]Address Correspondence to wei@chem.ufl.edu

Table of Contents

Page No.